

4-2016

Effect of humidity on the creep response of cellulose nanocrystals films

Marianne C. Valone
Purdue University

Follow this and additional works at: https://docs.lib.purdue.edu/open_access_theses

 Part of the [Materials Science and Engineering Commons](#)

Recommended Citation

Valone, Marianne C., "Effect of humidity on the creep response of cellulose nanocrystals films" (2016). *Open Access Theses*. 822.
https://docs.lib.purdue.edu/open_access_theses/822

This document has been made available through Purdue e-Pubs, a service of the Purdue University Libraries. Please contact epubs@purdue.edu for additional information.

**PURDUE UNIVERSITY
GRADUATE SCHOOL
Thesis/Dissertation Acceptance**

This is to certify that the thesis/dissertation prepared

By Marianne Catherine Valone

Entitled
EFFECT OF HUMIDITY ON THE CREEP RESPONSE OF CELLULOSE NANOCRYSTALS FILMS

For the degree of Master of Science in Materials Science Engineering

Is approved by the final examining committee:

Jeffrey Youngblood	_____	_____
<small>Chair</small>	_____	_____
John Howarter	_____	_____
Carlos Martinez	_____	_____
_____	_____	_____

To the best of my knowledge and as understood by the student in the Thesis/Dissertation Agreement, Publication Delay, and Certification Disclaimer (Graduate School Form 32), this thesis/dissertation adheres to the provisions of Purdue University's "Policy of Integrity in Research" and the use of copyright material.

Approved by Major Professor(s): Jeffrey Youngblood

Approved by: David Bahr 04/18/2016
Head of the Departmental Graduate Program Date

EFFECT OF HUMIDITY ON THE CREEP RESPONSE OF CELLULOSE
NANOCRYSTALS FILMS

A Thesis

Submitted to the Faculty

of

Purdue University

by

Marianne C Valone

In Partial Fulfillment of the

Requirements for the Degree

of

Master of Science in Materials Science and Engineering

May 2016

Purdue University

West Lafayette, Indiana

ACKNOWLEDGEMENTS

I would like to thank Professor Jeffrey P. Youngblood for his guidance and support during the past two years. I would also like to thank Professors Carlos Martinez and John Howarter for serving on my advisory committee. To Professor Carol Handwerker for guiding my studies in sustainability. To my parents for always believing in and supporting me in everything I do.

The work I have done would not have been possible without Shikha Shrestha, Shane Peng, Reaz Chowdhury, Nelyan Lopez-Perez, Logan Kearney, Youngman Yoo, Francisco Montes, Gamini Mendis, Kai Gao, and all my friends and colleagues I have made at Purdue.

I also want to thank the Forest Products Laboratory for providing the Cellulose Nanocrystals used for this work and providing the funding. And finally to Purdue University for providing the Knox Fellowship during my first year of my degree.

TABLE OF CONTENTS

	Page
LIST OF TABLES	v
LIST OF FIGURES	vi
ABSTRACT	vii
CHAPTER 1. INTRODUCTION	1
1.1 Cellulose Nanocrystals.....	1
1.1.1 Cellulose Nanocrystals Films	3
1.2 Creep.....	4
1.2.1 Maxwell Model.....	5
1.2.2 Kelvin-Voigt Model.....	6
1.2.3 Burgers Model	7
1.3 Dynamic Mechanical Analysis	8
1.4 Creep of Cellulose Nanocrystals.....	9
1.5 Humidity Effect on Polymer Films.....	10
CHAPTER 2. EXPERIMENTAL PROCEDURES.....	11
2.1 Materials	11
2.2 CNC Film Preparation	12
2.2.1 Self Organized Films	13
2.2.1.1 Variations of Self Organized Films	14
2.2.2 Sheared Films.....	14
2.3 Laser Cutter.....	15
2.4 Dynamic Mechanical Analysis	15
2.4.1 DMA Method.....	16
2.4.2 Variations of DMA Method.....	17
2.5 Optical Microscopy.....	18
CHAPTER 3. RESULTS AND DISCUSSION	19
3.1 DMA Results of 3.5 wt.% Films.....	19
3.2 DMA Results of 9.1 wt.% Films.....	22
3.3 Comparison of 3.5 wt.% and 9.1 wt.% Films	25
3.4 Optical Microscopy Images of 3.5 wt.% films	28

	Page
3.5 Optical Microscopy Images of 9.1 wt.% films	32
3.6 Comparison of 3.5 wt.% and 9.1 wt.% films Optical Microscopy Images.....	36
CHAPTER 4. CONCLUSIONS AND FUTURE WORK.....	37
LIST OF REFERENCES	39

LIST OF TABLES

Table	Page
Table 1. Approximate weight of CNCs used to make 3.5 wt.% and 9.1 wt.% films.....	12
Table 2. Slope changes for 3.5 wt.% films at 30°C and 50°C	19
Table 3. Slope changes for 9.1 wt.% films at 30°C and 50°C	22
Table 4. Average maximum strain and the time it took to reach this maximum at 50°C for 3.5 wt.% and 9.1 wt.% films	25
Table 5. Average maximum strain and the time it took to reach this maximum at 30°C for 3.5 wt.% and 9.1 wt.% films	26

LIST OF FIGURES

Figure		Page
Figure 1.	Maxwell Model for creep	5
Figure 2.	Kelvin-Voigt Model for creep	6
Figure 3.	Burgers Model for creep.....	7
Figure 4.	TEM Image coupled with Image J of Forest Products Laboratory Cellulose Nanocrystals.....	11
Figure 5.	Representation of CNCs + water solution being poured into a petri dish	13
Figure 6.	Graphs of the strain response of 3.5 wt.% films at 30°C (a) and 50°C (b) ...	21
Figure 7.	Graphs of the strain response of 9.1 wt.% films at 30°C (a) and 50°C (b) ...	24
Figure 8.	Micrographs of 3.5 wt.% films before (a) and after (b) humidity using non-polarized light	30
Figure 9.	Micrographs of 3.5 wt.% films before (a) and after (b) humidity using polarized light.....	31
Figure 10.	Micrographs of 9.1 wt.% films before (a) and after (b) humidity using non-polarized light	34
Figure 11.	Micrographs of 9.1 wt.% films before (a) and after (b) humidity using polarized light.....	35

ABSTRACT

Valone, Marianne C. M.S.M.S.E., Purdue University, May 2016. Effect of Humidity on the Creep Response of Cellulose Nanocrystal Films. Major Professor: Jeffrey P. Youngblood.

Cellulose nanocrystals (CNCs) are a derivative of cellulose, the Earth's most abundant source of a sustainable polymer. There are many applications for CNCs such as batteries, antimicrobial films, flexible displays and drug delivery. This research is focused on CNCs films and the mechanical properties once humidity was introduced.

The creation of self-aligned CNCs films was utilized to perform dynamic mechanical analysis (DMA) testing. The Forest Products Lab (FPL) in Madison, Wisconsin provided the CNCs used. Both 3.5 wt.% and 9.1 wt.% films were made and tested. A DMA method was created to test the creep response of the CNCs films at humidity levels of 80%, 40% and 0%. This method was performed at both 30°C and 50°C. Before and after the films were tested in the DMA, optical microscopy images were taken to analyze the structure of the films. It was found that the films experienced a higher strain rate at 30°C, but regardless of temperature the trend of strain was non-linear, with the highest strain reached at 80% humidity. There was full creep recovery at 40% humidity and shrinkage of the films once the humidity level reached 0%.

CHAPTER 1. INTRODUCTION

1.1 Cellulose Nanocrystals

Cellulose is the most abundant renewable natural organic compound on Earth comprising about 33 percent of all vegetable matter. It can be found in a multitude of sources including plants, algae, tunicates, and certain species of bacteria. Cellulose nanocrystals (CNCs) are the primary structural unit extracted from the mentioned sources. The methods of extraction can either be chemical or mechanical to separate the crystalline phase from the bulk cellulose [1]. These techniques include acid hydrolysis [2], TEMPO-mediated oxidation [3], [4] and homogenization and grinding [5], [6]. The CNCs provided from the Forest Products Laboratory (FPL) for this research were extracted from bulk cellulose by acid hydrolysis.

CNCs have a rod-like shape with the dimensions varying depending on source i.e., 3-20 nm wide by 100-2000 nm long [7]. Although difficult to measure individual CNCs, when together they offer many advantages opposed to just being renewable and sustainable. CNCs have high tensile strength, 7.5 GPa and high elastic modulus, 110-220 GPa in the axial direction and 10-50 GPa in the transverse direction [8]. They also have low coefficient of thermal expansion [9], easy orientability under shear [9], [10], refractive index on par with most polymers [11] and uniform prismatic dimensions [12]–[14]. Since the cost of cellulose nanocrystals is lower than other nanomaterials, such as carbon nanotubes [15], they are desirable fillers for polymer matrix composites (PMCs). However, there are still some problems with using CNCs as fillers due to their hydrophilic nature and large interfacial attraction [1].

Cellulose nanomaterials are renewable and offer high mechanical properties, hence they are able to offer an alternative to traditional petroleum-based plastics in different fields of study. The applications include batteries, antimicrobial films, flexible displays and drug delivery [12]. These applications depend on the alignment of the CNCs, which will change the optical, mechanical and thermal properties. Many mechanical properties have already been discovered, however the effect of humidity on the creep of these CNCs has not. The following research will describe the creep response when humidity is introduced to CNC films.

1.1.1 Cellulose Nanocrystals Films

Cellulose Nanocrystals are used to create films for many types of applications that will be explained in this section. One of the applications involves creating recyclable organic solar cells on cellulose nanocrystals substrates. One advantage of creating solar cells on CNC substrates is the sustainability and recyclability. The film and substrate are able to swell and once the water evaporates away, the CNC is left for recovery. Then the components of the solar cell are allowed to separate. Although these solar cells are not fully optimized yet, the research is promising as the power conversion efficiency reaches to 2.7%. This is encouraging for the technology, which is headed towards sustainability [16].

CNCs are low in toxicity and ecotoxicological risk, which has led to recent developments for tissue engineering. In tissue engineering, dense films are relevant in skin tissue engineering as well as preventing tissue adhesions in surgeries involving soft tissue and regenerative medicine [17]. Although neat CNC films are not useful by themselves for tissue engineering, adding CNCs for reinforcement to collagen-based composite films is an alternative. This increased the mechanical properties and the stability, which led to an increase in swelling capacity, a desirable characteristic for tissue engineering [18].

Polymer films are also used for food packaging applications. However, drawbacks of using non-synthetic polymers include the lack of degradability, recyclability and the high carbon footprint. There are multiple synthetic biodegradable polymers, such as polyhydroxybutyrate (PHB) that have been developed that could be used for the food packaging industry [19]. However, PHB is highly brittle, with poor mechanical and gas barrier properties. These properties are critical for food storage [20]. Combining PHB with cellulose will improve the gas barrier properties of the polymer and lead to further food-packaging applications [21]. These are the variety of applications CNCs films possess. Further mechanical testing, such as creep response, need to be analyzed to expand the applications and uses of these films.

1.2 Creep

When testing for mechanical properties of polymers, there are two types of testing: static and transient. With regards to transient testing, there are two distinct measurements that can be used: stress relaxation and creep. These measurements help to characterize the material that is being tested. Stress relaxation measures the stress required to hold a specimen at a fixed elongation with constant temperature. Stress and the stress relaxation modulus are both functions of time. However, the research that will be explained in the following chapters looked at the creep response to humidity while experiments were run in the DMA. Creep test results are good for selecting a polymer or material that must sustain loads for long time periods. A typical creep test is one in which the stress is held constant and the strain is time dependent. During the creep test three different responses may be observed: ideal elastic, ideal viscous and viscoelastic. Viscoelastic materials have both viscous and elastic characteristics. These types of materials are able to have full recovery due to the elastic property. However, the recovery is delayed because of the viscous influence. Typically, a dashpot is used as the viscous element while an ideal spring is used as the Hookean, or elastic, element for mechanical models. The spring measures the elastic modulus of the material while the dashpot measures the viscosity. There are multiple different creep models available to analyze viscoelastic materials, which include Maxwell, Kelvin-Voigt, and Burgers Models [22]. In the following sections, these three models will be explained in detail.

1.2.1 Maxwell Model

The Maxwell Model is where the spring and dashpot are in series together as seen in Figure 1.



Figure 1. Maxwell Model for creep.

Since the two elements are in series with one another, the total strain is actually the strain of each individual element added together. The equation to determine strain rate using a Maxwell is seen in Equation 1.

Equation 1

$$\frac{\partial \varepsilon}{\partial t} = \left(\frac{1}{E}\right) \frac{\partial \sigma}{\partial t} + \frac{\sigma}{\eta}$$

However, as stated previously, creep has a constant stress, which is applied instantaneously. This means the creep compliance, $D(t)$ can be written as follows in Equation 2 [22].

Equation 2

$$D(t) = \frac{\varepsilon(t)}{\sigma_0} = \frac{t}{\eta} + \frac{\varepsilon_0}{\sigma_0} = \frac{t}{\eta} + D$$

1.2.2 Kelvin-Voigt Model

Unlike the Maxwell Model, the Kelvin-Voigt Model is where the spring and dashpot are in parallel as seen in Figure 2.

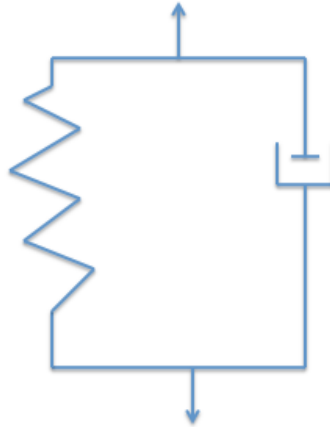


Figure 2. Kelvin-Voigt Model for creep.

For this model, the strain on the two elements must be the same, but now the stresses are combined. Thus the following equation shows the fundamental relation for this model.

Equation 3

$$\sigma = E\varepsilon + \eta \frac{\partial \varepsilon}{\partial t}$$

As for determining the creep deformation, Equation 4 is used.

Equation 4

$$D(t) = D \left[1 - \exp\left(\frac{-t}{\tau}\right) \right]$$

There are advantages and disadvantages of using either the Maxwell or Kelvin-Voigt Model. If more interested in getting information about the modulus of a model, Maxwell better represents this. However, if compliance is needed, Voigt is the model to use.

These two models only give results for one transition opposed to multiple transitions. Due to this, there are creep models used for multi-element materials [22].

1.2.3 Burgers Model

One multi-element model is the Burgers Model. This model combines the previous two explained models together in series as seen in Figure 3 [23].

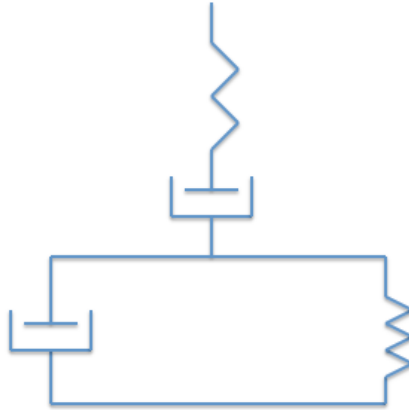


Figure 3. Burgers Model for creep.

This model separates the strain into three types of deformation: instantaneous, elastic and plastic. Together the equation to determine the strain can be seen in Equation 5 [24].

Equation 5

$$\varepsilon(t) = \frac{\sigma}{E_E} + \frac{\sigma}{E_{VI}} \left[1 - \exp\left(-\frac{tE_{VI}}{\eta_{VI}}\right) \right] + \frac{\sigma}{\eta_{VP}} t$$

These different models of creep can be analyzed through different methods using the dynamic mechanical analysis (DMA).

1.3 Dynamic Mechanical Analysis

Dynamic mechanical analysis (DMA) is one of the basic tools used to measure the viscoelastic properties of polymers. The viscoelastic properties can be related to temperature, time, frequency, or even humidity if the relative-humidity chamber is placed on the equipment. Different transitions and bulk properties of polymers can also be analyzed by the DMA. The responses of materials placed in the DMA are measured by applying an oscillating force to the material. Stress, the measure of force applied to an area, and strain, the deformation of a sample, are the two most important concepts of DMA. By obtaining these different mechanical properties, the performance of materials in different applications can be projected. Since DMA relies on stress and strain, both creep-recovery and dynamic tests can be performed on materials [25].

Research has been done in the past on the creep response of different polymeric materials using the DMA. Previously, the creep response of wood had been studied when exposed to different temperatures and moisture content [26]–[28]. In one study, the temperature range varied from 5°C to 105°C while the moisture content varied from 0% to over 30%. As the temperature increased, the instantaneous compliance increased regardless of the moisture content. Comparatively, the instantaneous compliance at the same temperature also increased as the moisture content was increased. Moisture content and temperature effect the mechanical properties of pieces of wood [26].

In another study, many different types of wood were tested at varying moisture contents to determine the effect with regards to the viscoelasticity. The woods tested were then divided into two groups after the testing. Birch-like woods showed a response that there is an effect in viscoelasticity when there is a variation in moisture content. On the other hand, spruce-like woods showed the change in moisture content and temperature does not change the creep strain response [28].

1.4 Creep of Cellulose Nanocrystals

There have not been many studies done on finding the creep response of individual CNCs. However, there have been some studies on the creep response of PMCs with CNCs added as fillers. One reason CNCs are added is to enhance the creep performance of composite matrices. This is because fillers have tendency to add a more solid-like response that leads to a reduced creep deformation compared to neat-composites [29]–[34]. When CNCs were added to low-density polyethylene (LDPE) and polypropylene (PP), there was a change of the creep deformation. Neat LDPE and PP both showed non-linear deformation with time. Composites with both 5% and 10% CNCs were created with LDPE and PP. After just 30 minutes, neat-LDPE showed 29% deformation, while the composites with CNCs showed a deformation of 25% for 5% CNCs and 17% for 10% CNCs. Neat-PP showed a creep deformation of 48% after 30 minutes, while the composites with 5% CNCs showed 31% deformation and 27% deformation for 10% CNCs. These results show that CNCs can improve the effective of the stress transfer between the polymer and filler which enhances the creep performance of PMCs [1].

In another study, composite films created with CNCs and polyurethane (PU) were created to test for shape memory properties. Typical shape memory polymers have a low stiffness compared to metals and ceramics, which is why CNCs were added as fillers. These PMCs did show a higher tensile modulus and strength than those without the CNCs as fillers. Also there was an elongation seen at the break of the film. The creep deformation decreased when the CNCs concentration increased. Although the modulus and strength were increased with the CNCs, there was not a substantial effect on the recovery of the shape memory as this behavior still is controlled primarily by the PU properties [35].

1.5 Humidity Effect on Polymer Films

The effect of humidity and other environmental conditions on polymer films have been studied previously [36], [37]. In one study, it is seen that there is a non-linear relationship between the environmental conditions and equilibrium moisture content. This research was done on polyurethane lacquer, a synthetic polymer. The water absorption acts as a plasticizer in PU lacquers. These films have a complex dependence on different environmental conditions, such as UV irradiation and water absorption. With regards to the water absorption, the films show an increase in maximum strain [36].

Another study shows the effect of humidity on nonelectrolyte polymer films versus polyelectrolyte multilayer films (PEMs). The nonelectrolyte polymer films exhibit minimal changes in mechanical properties when introduced to humidity. However, PEMs show a substantial responsiveness with regards to humidity. The films swelled when introduced to humidity. This study demonstrated the humidity-dependent changes of thickness and Young's modulus of PEMs, and how changing the environmental conditions can change the mechanical properties [37].

Previous research has shown the impact of CNCs as fillers in PMCs and the creep response of these matrices. However, the creep response of neat-CNC films has not been studied. The following research will discuss neat-CNCs films creep response when introduced to different humidity levels.

CHAPTER 2. EXPERIMENTAL PROCEDURES

2.1 Materials

The University of Maine Process Development Center in collaboration with the Forest Products Laboratory (FPL) in Madison, Wisconsin provided the cellulose nanocrystals (CNCs) that were studied for this research. The solids in the batch were 11.8 wt.% CNC in water. This was formed by acid hydrolysis of 1 wt.% sulfur on dry CNC sodium. These CNCs have an aspect ratio of 9.5, with a length of 64 ± 5 nm and width of 7 ± 1 nm. Figure 4 shows the TEM image coupled with Image J of the CNCs.

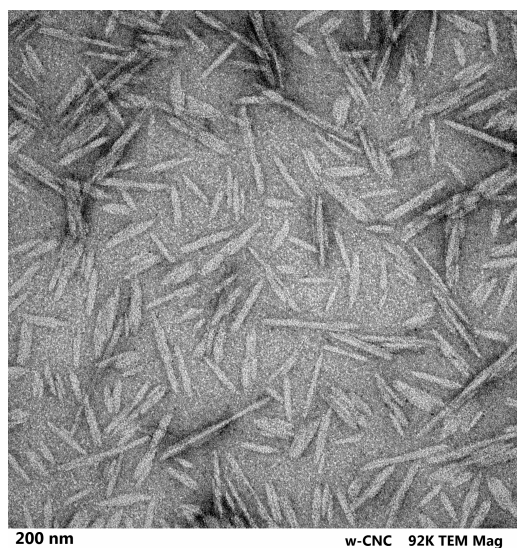


Figure 4. TEM Image coupled with Image J of Forest Products Laboratory Cellulose Nanocrystals.

The CNCs were combined with Nanopure water from the lab at different weight percentages of 3.1 and 9.5, which will be explained in detail in Section 2.2.

2.2 CNC Film Preparation

In a beaker, the amounts of CNC and Nanopure water were combined. The amount of CNC is determined by the following equation with the remaining weight being the amount of water needed.

Equation 6

$$\text{weight of stock CNC} = \frac{\text{total weight} \times \text{CNC percent desired}}{11.8 \text{ wt}\%}$$

After many failed attempts of making films, it was determined that to obtain the correct thickness, the total weight must increase for lower percentages of CNCs. This was to ensure that the thicknesses of the 3.5 wt.% and 9.1 wt.% films were the same. Shown in Table 1 are the approximate amounts of CNC used to obtain a film that is approximately 100 micrometer (μm) thick. The thickness was measured using a micrometer in 5 different parts of the film and averaging the thicknesses together.

Table 1. Approximate weight of CNCs used to make 3.5 wt.% and 9.1 wt.% films.

Weight Percent of CNC	Total Weight	Weight of CNC	Thickness of Film
3.5 wt.%	55 g	16.31 \pm 0.05 g	100 \pm 2 μm
9.1 wt.%	30 g	23.14 \pm 0.05 g	100 \pm 2 μm

After the amounts of CNC and water were combined in a beaker, the solution was sonicated in the Branson Digital Sonifier. This was done at amplitude of 40% for three minutes with the pulse on for one second and off for one second. These were the settings that worked best for the 3.5wt% solutions. However, the 9.1wt% solutions had much more solid than liquid as seen in Table 1. Due to this, the solution was placed in the Sonifier for twice as long to ensure a total dispersion, or transparency of said mixture.

Once the ultrasonications were completed, two different types of films were attempted: self-organized and sheared. The processes for making these types of films will be discussed in the following sections.

2.2.1 Self-Organized Films

In order to make self-organized films, petri dishes made of glass and polystyrene (PS) were used. This was done to compare the differences between the films. The previously ultrasonicated solution was poured into a petri dish as seen in Figure 4. These filled petri dishes were then left in a cabinet to dry at room temperature.

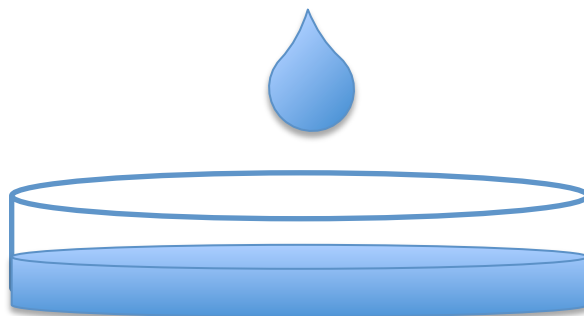


Figure 5. Representation of CNCs + water solution being poured into a petri dish.

They still had access to air flow by keeping the cabinet door slightly open at all times during the drying process. The lower CNC weight percentages took longer to dry due to the increase in the amount of water left to evaporate. The 9.1wt% CNC films took around three to four days to dry, while the 3.5wt% CNC films took around seven to nine days to dry [9], [10].

The total amount of weight of the solution played an important role in determining the outcome of the drying process. If there were too much solution in the petri dish, the films would tend to crack in the middle. However, if there were not enough solution, the films would be too thin to remove from either the glass or plastic dish. Hence, a higher total volume for lower weight percentages and a lower total volume for higher weight percentages of CNCs. The films prepared in glass petri dishes were much easier to

remove without cracking rather than the films prepared in PS petri dishes. Moving forward, only the films made in glass petri dishes were used for mechanical testing.

These films are considered self-organized because during the drying process, the cellulose nanocrystals self-align randomly. This will be further analyzed in Sections 3.5-3.7 where the microstructures are examined from optical images.

2.2.1.1 Variations of Self-Organized Films

Other experiments were attempted to create films to discover if there were any variations. The ultrasonicated solution was placed into the refrigerator for 24 hours before being poured into the petri dish. This experiment proved to not have an impact on the types of films that were made post-drying. Thus, it was not used to carry on the process of making films.

Another variation was using different weight percentages of CNCs to create films. Films with a lower weight percentage of CNC, around 1.6, did not form films that could be tested in the DMA as the films were either too brittle, too thin, or unable to be removed from the petri dish. The other attempt made was to make the films with higher weight percentage than 9.1 wt.%, but it did not work and hence it was determined that 9.1 wt.% was the maximum limitation.

2.2.2 Sheared Films

As previously stated, sheared films were attempted for testing. After the sonication process was complete, the solution would be placed on both glass and polyethylene terephthalate (PET) substrates. It was determined that the films were best made on the PET substrate because the solution would not stay in the designated area on the glass substrate due to the hydrophobicity of the glass being used. Small amounts of solution were placed on the substrate at a time and then sheared down a designated area with a

small razor blade multiple times. This process continued until the entire solution was sheared. These sheared films were left to dry uninterrupted for a few days. However, as the films were drying the thickness would vary throughout. The film would tend to be thicker in the middle of the film and very thin on the outside, making the film “curl-up” on the edges. Not only would there be a variation in thickness but in many areas, the film would also crack throughout the film. Since the film was various thicknesses and cracking in the thicker areas, the films were unable to be cut into samples for mechanical testing. Also, the CNCs were not well dispersed once the film was dried compared to the initial process of shearing [9], [10].

Because of these reasons, it was decided to proceed with only the unsheared films for further testing.

2.3 Laser Cutter

Once the films were completely dried, they were taken to the Birck Nanotechnology Center to cut into numerous samples. The Universal Laser Systems PLS6MW Multi-Wavelength Laser Cutter was used. The samples were cut into 4 mm x 15 mm samples. This was to ensure that the samples were long enough in case they were broken in the process of placing into the dynamic mechanical analysis. Afterwards, the experiments in the DMA were able to start.

2.4 Dynamic Mechanical Analysis

A TA Instruments DMA Q800 was used for the majority of this research. The DMA-Relative Humidity accessory was placed on the instrument before any calibration was conducted. First the position was calibrated and then the film tension clamp was performed. After both calibrations were complete, the DMA was ready to be used to start testing the self-aligned films.

2.4.1 DMA Method

The main method of this research was done under a controlled force using the film tension clamp. The process started by applying an initial force of 0.001 N exerted onto the film. The samples were ran at the temperatures 30°C and 50°C, and at relative humidity levels 80%, 40% and 0%. The method is as follows:

1. Data Storage On
2. Equilibrate at 30/50°C
3. Relative Humidity 80%
4. Isothermal 50 minutes
5. Ramp Stress 0.5 MPA/min to 1 MPA
6. Isothermal 180 min
7. Force Ramped to 0.4 N
8. Isothermal 180 min
9. Humidity 40%
10. Isothermal 25 min
11. Repeat Steps 5-8
12. Humidity 0%
13. Isothermal 25 min
14. Repeat Steps 5-8

This method was approximately 20 hours per run, indicating that each sample was in the DMA for around 40 hours. Some films did not make it through the entire run which could be due to either human error, not tightening the clamp enough to make sure the film did not slip during the run, or failure in the film, the film was too brittle to withstand

the amount of humidity and stress placed on the film. During these runs it was found that most of the films tested using this method did not fail during the 30°C or 50°C run. The isothermal times were chosen due to the increase or decrease amount of humidity level. At the beginning of the experiment, the humidity is increased from 0% to 80%, thus 50 minutes was chosen. When the humidity levels were decreased to 40% and then to 0%, only 25 minutes was chosen, as the decrease was half the amount from the initial increase of humidity. It took longer for the humidity chamber to increase to 80% than it did to decrease to 40% and then 0% levels.

2.4.2 Variations of DMA Method

Before the success of this particular method, other methods were first run that did not work well with the thin, brittle films. One of the first methods attempted was starting at 0% humidity and working up to 80% humidity. However when this method was used, most samples seemed to break well before the 30°C experiment was complete. This may have been due to the brittleness of the films. Since the films used were just 100 μm thick, the intensity and length of the method may have been too much. This is why the method chosen begins with increasing the humidity directly to 80% at the beginning of the experiment after the temperature was set.

Once this was determined to work better for the unsheared CNC films, the next thing that needed to be done was to determine how long each part of the method should run. Since this research is to discover if humidity has an effect on the creep of CNC films, the method needed to be long enough at the different humidity levels to make sure there was not a change as the different humidity levels were stabilized. This is particularly seen in steps 6 and 8 of the method used. These steps are isothermal for 180 minutes. Three hours was chosen because this would be long enough to see any change that may occur as the film is at 80, 40 and 0 percent humidity. This meant that the film would be under each humidity level for approximately 6 hours after the certain humidity was stabilized. Before 180 minutes was determined, 60 minutes and 120 minutes were used for both

steps 6 and 8. Sixty minutes for steps 6 and 8 proved to not be long enough to see if any real change would occur. 120 minutes also seemed to be just shy of the minimum amount of time needed for each step. Thus, 180 minutes was finally determined to be the best to see the creep response.

2.5 Optical Microscopy

Before and after the films were tested in the DMA at 30°C and 50°C, optical images were taken by using optical microscope, Carl Zeiss with Canon EOS Rebel T5i camera. The optical images of the microstructure were taken using both non-polarized and polarized light. In Sections 3.5-3.7, the micrographs before and after humidity effect will be compared, as well as the 3.5wt% versus the 9.1wt%.

CHAPTER 3. RESULTS AND DISCUSSION

3.1 DMA Results of 3.5wt% Films

The data from the DMA for 3.5wt% films are shown in Figure 5, at temperatures (a) 30°C and (b) 50°C. Five samples were used to determine an average strain. One of the first differences observed between the two graphs is the strain rate as the humidity is ramped to 80% at the beginning of the experiment. At 30°C, the strain is not able to increase at a steady rate or normalize once the force begins to rise. However at 50°C, the strain does appear to increase at a steady rate when the humidity is increased to 80% and levels out as the force is held at 0.4 N. Table 2 displays the differences between the slopes at the two temperatures when humidity is changed. At 50°C, the strain increases at a much faster rate than at 30°C.

Table 2. Slope changes for 3.5 wt.% films at 30°C and 50°C.

Humidity Change	Slope for 30°C	Slope for 50°C
0% to 80%	0.018 ± 0.002	0.026 ± 0.001
80% to 40%	-0.022 ± 0.001	-0.042 ± 0.002
40% to 0%	-0.010 ± 0.001	-0.013 ± 0.002

The first zoomed in section at 30°C shows that the strain actually increases as the force is brought back to 0 N from 0.4 N. It was expected that the strain would always decrease at this part of the system at 80%, 40% and 0% humidity levels. This is shown in the zoomed in section at 50°C in Figure 5b. Here the strain decreases at a constant rate that is actually seen at all three humidity sections when the force is ramped back to 0 N.

Although the strain has a more difficult time increasing at 30°C than at 50°C, during the 30°C run the samples go to a higher strain percentage just at a slower rate. At 30°C the highest strain achieved is 2.16% at 414.73 minutes, whereas at 50°C the highest strain reached is 1.53% at 257.26 minutes. This shows that the films' response to creep at 80% humidity are higher, but slower at 30°C and faster and lower at 50°C.

In the second zoomed-in section Figure 5a at 30°C where the humidity is changed from 80% to 40%, the strain is decreasing at a rate that ends halfway through the force stabilized at 0.4 N. When compared to the results at 50°C, the strain decreases slower at 30°C. In the 50°C graph 5b, the strain decreases almost at the same rate (Table 2) as the humidity is decreasing and is more stabilized as the force is ramped. However in both graphs, there is almost a full creep recovery for both samples as the strain is close to 0% at this point. The reason that it could take longer to see the strain level out as the force is stabilized is due to the higher strain achieved initially when under 30°C.

Finally, the third zoomed-in picture in Figure 5a shows the change of strain right before the force is decreased at 0% humidity. Although this is closer to the trend that was expected, it does not exactly match up to the trend at 50°C. Although during both conditions, the strain decreases at a slower rate than from 80% to 40%, 50°C decreases its strain at a bit faster of a rate. In this section the films go from complete creep recovery response to shrinkage. The films under 30°C shrink more than the films at 50°C.

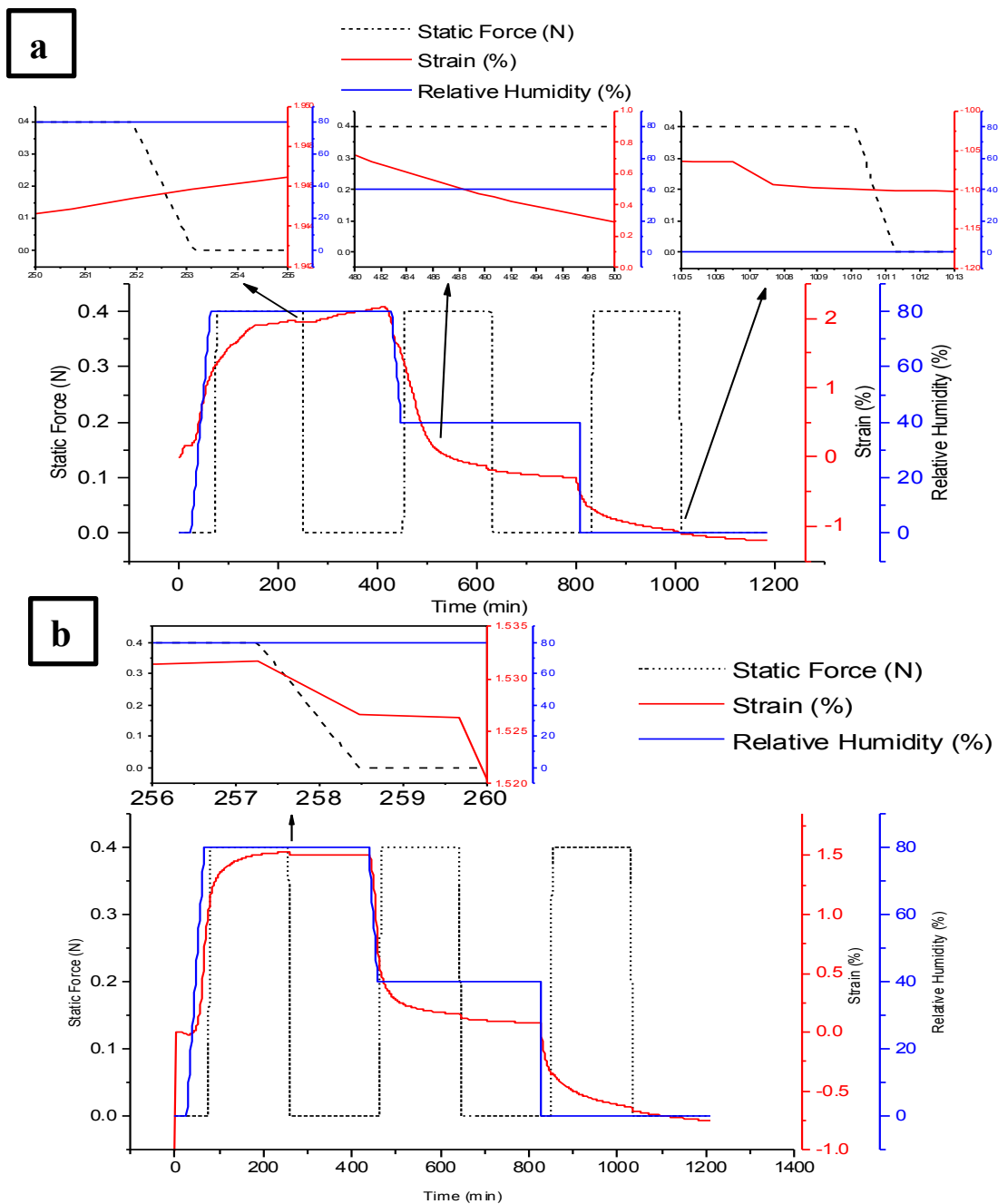


Figure 6. Graphs of the strain response of 3.5 wt.% films at 30°C (a) and 50°C (b). (a) shows zoomed in regions when the force is brought back to 0 N at 80%, 40% and 0% humidity levels. (b) shows a zoomed in region when the force is brought back to 0 N at 80% humidity to depict the change that occurs at all 3 humidity levels.

3.2 DMA Results of 9.1 wt.% Films

The data from the DMA for 9.1 wt.% films are portrayed in Figure 6, at temperatures (a) 30°C run and (b) 50°C. Just as said for the 3.5 wt.% films, there were multiple samples were used to calculate an average strain. Once again, the 30°C samples seem to have a difficult time reaching the highest strain at 80% humidity at a steady rate. There is also the issue of the strain not stabilizing as the force is increased to 0.4 N as it does in 6b. During the runs with this weight percentage of film, the strain reaches its maximum strain at 2.79% at 361.32 min for 30°C and 1.43% at 245.10 for 50°C. Displayed in Table 3, it again took longer at the lower temperature to increase to its maximum strain compared to the rate at 50°C. Even though it took longer to reach the maximum strain for 30°C, the films responses to creep at 80% humidity are higher than those experienced at 50°C.

Table 3. Slope changes for 9.1 wt.% films at 30°C and 50°C.

Humidity Change	Slope for 30°C	Slope for 50°C
0% to 80%	0.013 ± 0.001	0.026 ± 0.001
80% to 40%	-0.026 ± 0.002	-0.028 ± 0.001
40% to 0%	-0.006 ± 0.002	-0.014 ± 0.001

The first zoomed in section in Figure 6a shows the strain is increasing as the force is ramped back down to 0 N. Again, it was anticipated that the strain would always decrease with the force decreasing. This trend is shown at the zoomed in section at 50°C in Figure 6b. The strain is decreasing at a constant rate at all three humidity levels for this temperature.

In the second zoomed in section at 30°C, the humidity is at 40%. Here, the strain actually decreases halfway through the stabilization of the force at 0.4 N. It is interesting to observe this as the initial decrease in strain went at about the same rate as in the 50°C run. However there was not full creep recovery at 30°C until the end, whereas there was almost total creep recovery as the humidity was ramped down. Yet again, it may have

taken longer to reach total creep recovery at the lower temperature as it had initially reached a higher strain percentage at 80% humidity.

Finally, the third zoomed in picture at 30°C Figure 6a shows the decrease in strain starting before the force is decreased at 0% humidity. This is the closest to the trend that was expected and seen at 50°C. For both temperatures, the strain decreases at a much slower rate than previously. When the humidity is decreased to 0% and normalized for the duration of the experiment, the films go from complete creep recovery to shrinkage. The films under 30°C shrink more than the films at 50°C, just like it was observed for 3.5wt% films.

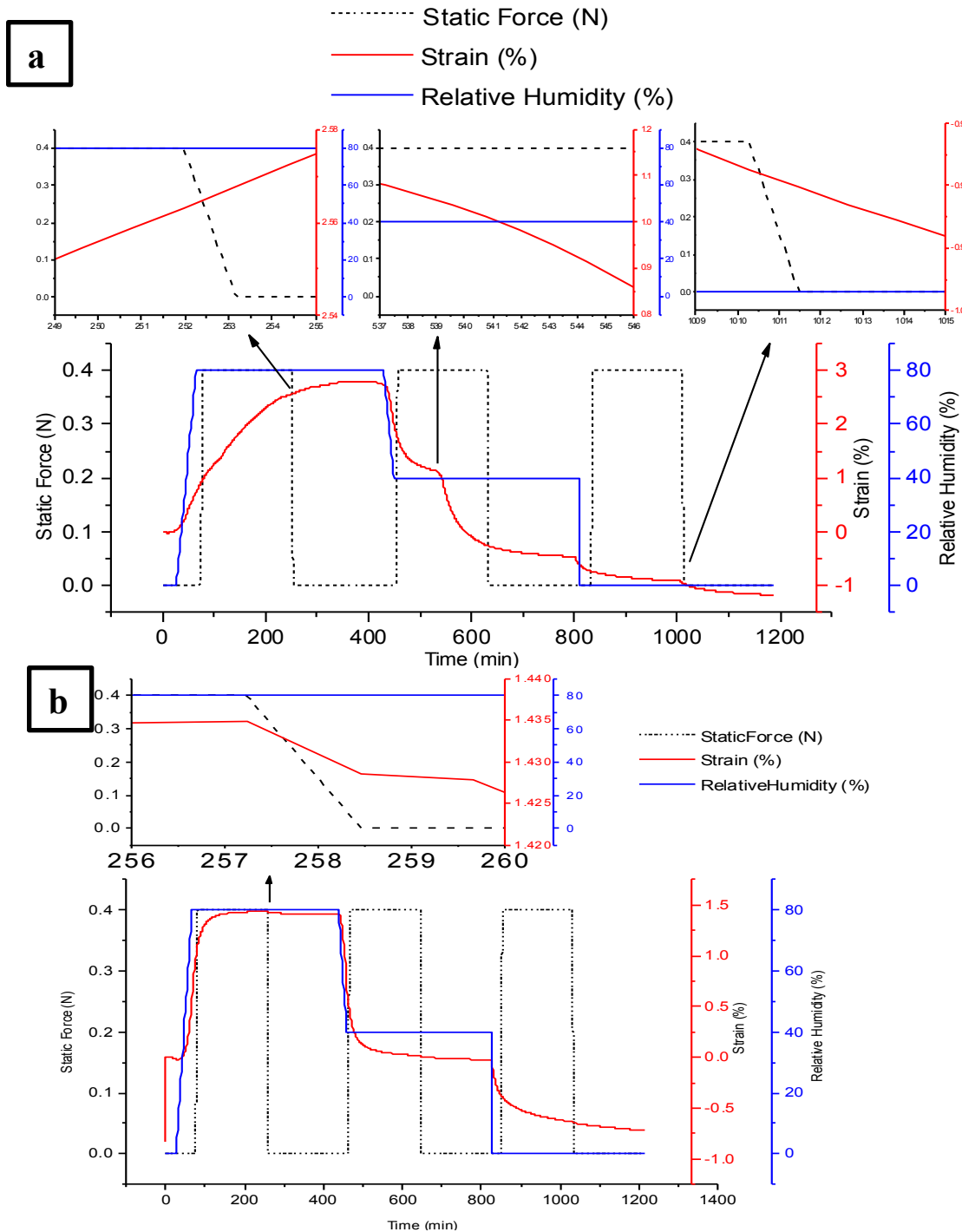


Figure 7. Graphs of the strain response of 9.1 wt.% films at 30°C (a) and 50°C (b). (a) shows zoomed in regions when the force is brought back to 0 N at 80%, 40% and 0% humidity levels. (b) shows a zoomed in region when the force is brought back to 0 N at 80% humidity to depict the change that occurs at all 3 humidity levels.

3.3 Comparison of 3.5 wt.% and 9.1 wt.% Films

In the previous sections the DMA data was compared solely between the weight percentages of films individually. Here, the differences between 3.5 wt.% and 9.1 wt.% films will be analyzed.

The trends are the same regardless of the weight percentage of CNC at 50°C. The main differences at this temperature are the strain rate when the humidity is decreased to 40% from 80% and the maximum strain experienced during the runs. The trends are suspected to be the same because the humidity effect during the 30°C run erased the drying and thermal histories of the films. This means that now the films are basically equivalent regardless of the weight percentage of cellulose nanocrystals. They are acting the same and as a typical polymer film. The results are shown below in Table 4.

Table 4. Average maximum strain and the time it took to reach this maximum at 50°C for 3.5 wt.% and 9.1 wt.% films.

Film Concentration	Average Maximum Strain	Time
3.5 wt.%	1.53% ± 0.16	257.26 min
9.1 wt.%	1.43% ± 0.13	245.10 min

As for the other major difference at 50°C, the strain rate for the 9.1 wt.% films was slower as the humidity decreased from 80% to 40%. These values can be compared in Table 4. It is possible that having a higher concentration of CNC in a film makes the creep recovery response a bit slower as there is more CNCs in the film than those of the 3.5 wt.% films. One way to test this theory would be by performing further experiments using different weight percentages that are lower and higher than 3.5 wt.% and see if the trend stays the same.

Although the 3.5 wt.% films had a slightly higher maximum strain at 50°C, the 9.1 wt.% films had a higher maximum strain at 30°C. This can be seen in Table 5. The higher

weight percentage of CNCs films not only experienced a higher maximum strain, but also at a faster time than the lower weight percent. The 9.1 wt.% films experienced the maximum strain almost an hour before the 3.5 wt.% films experienced the lower maximum percentage. Since the 9.1 wt.% films dried rather quickly, the cellulose nanocrystals did not have a lot of time to self assemble in a thermodynamically favorable way. Because of this, there was a high amount of residual stress in these films. With higher residual stress comes a higher strain as the initial force is admitted to the film. The 3.5 wt.% films took much longer to dry, thus there was time for the CNCs to self assemble in a thermodynamically favorable way. There was less residual stress in the films, leading to a lower maximum strain than the 9.1 wt.% films.

Table 5. Average maximum strain and the time it took to reach this maximum at 30°C for 3.5 wt.% and 9.1 wt.% films.

Film Concentration	AverageMaximum Strain	Time
3.5 wt.%	2.16% \pm 0.12	414.73 min
9.1 wt.%	2.79% \pm 0.13	361.32 min

Unlike at 50°C, the strain rates were very similar during the humidity changes for the 30°C runs at each weight percentage. Still, the 30°C results are not the best and in the future, experiments at higher temperatures need to be ran to compare the results for different weight percentages of CNC films.

Regardless of the temperature or weight percent of film used, one trend remained the same throughout every run. The largest strain experienced happened at 80% humidity, however the trend is non-linear when reducing in temperature. As the humidity was ramped up at a fast rate, the strain did as well. This is also seen in Niinivaara, et al. study of water uptake on CNCs films through quartz crystal microbalance with dissipation monitoring (QCM-D) experiment. In their experiment, ultrathin CNCs films were prepared using a spin coater. Different masses of CNCs were used to determine if there were a difference in the change of thickness (Δt) as the humidity was increased to 100%

and then brought back to 0%. In this, the trend is also non-linear. There is an increase in Δt as the humidity was increased [38]. This can be related to the increase in strain of the CNC films used for the experiments done in the DMA.

In Niinivaara, et al. study, the change of Δt from 80% to 40% humidity versus 40% to 0% humidity is comparable to the results found in Figures 5 and 6 from the DMA. From 80% to 40% humidity, there is a larger change in percent of strain or Δt than the change between 40% and 0% humidity. Just as stated previously about the films experimented on in the DMA, the films have experienced an increase with full recovery and in the end some skringage by the end of the experiment. Although the QCM-D and DMA do not report exactly the same data, the two experiments are complementary to the response of creep when humidity is introduced to CNCs films.

3.4 Optical Microscopy Images of 3.5 wt.% Films

Micrographs of 3.5 wt.% films were taken before and after the DMA experiments were conducted. Both non-polarized (Figure 7) and polarized (Figure 8) light were used to determine what changes happened to the films once exposed to humidity, stress and strain. Figures 7a and 8a show the film before humidity exposure while Figures 7b and 8b show the film after humidity is introduced to the film at both 30°C and 50°C. The non-polarized micrographs do not see much differences when compared.

Contrasting to the non-polarized images, the polarized micrographs show a difference in the vibrancy of the colors that appear. Before the films are exposed to the humidity, the colors are very distinct and vibrant, with more shades of blue appearing. After humidity, the colors are duller with more shades of yellow and red emerging. This could be due to the pitch length of the CNCs. CNC dispersions typically form in a chiral nematic structure. The characteristic repeat distance between the rod-like chains twisting around is described as the pitch-length [39]. This ordering of CNCs chains leads to the vibrant colors seen in polarized optical images of thin CNCs films.

CNC dispersions also exhibit lyotropic chiral nematic behavior at lower concentrations as they have lower viscosities and form in a shorter amount of time. Security features and the cosmetics industry have been attracted to these thin CNC films and their vivid iridescence. These colors can be tailored in many different ways: adding salt to increase the ionic strength to lead to a blue shift [40], ultrasonication of the dispersion to lead to a red shift [41], and by changing the temperatures the films are exposed to as higher temperatures also lead to a blue shift [42]. Different research groups, such as Kelly and collaborators at the University of British Columbia have started studying the development of these films and changing the birefringences of the CNC films. This group in particular studied mesoporous materials that incorporated CNCs. However, the humidity and creep effect of neat-CNC films birefringence have not previously been studied and will be analyzed in the coming sections.

A typical structure of CNCs exhibit a long pitch-length, however referring back to Section 2.2, the CNC and water solutions were ultrasonicated. Ultrasonication changes the chirality of the polymer chains by changing the pitch length. When this is done, the critical concentration needed for phase separation is increased. At higher weight percentages of CNCs, the pitch length may in fact increase as seen in Beck's study of CNC films. However, at the lower concentrations of CNCs, the chains are broken up which lead to a blue shift in the non-polarized films. As the films dried, the CNCs had the ability to self-organize freely as the pitch length was shorter. However, once the films were placed in an atmosphere with humidity and temperature, the CNCs pitch length may have possibly changed again. This could explain the differences in the two polarized images. When the films are under humidity, the CNC chains may start to overlap and stack on top of each other so the color is not as vibrant. Also, as the films are placed in higher temperatures the pitch length also increases. An increasing pitch length leads to a more red shades of colors. There have been previous studies that show the influence of temperature on the chiral nematic structure of cellulose [43]–[45]. Although most of these studies involve the temperature during the drying of the CNC films [42], the results show there is a change when the films are introduced to different temperatures in the DMA.

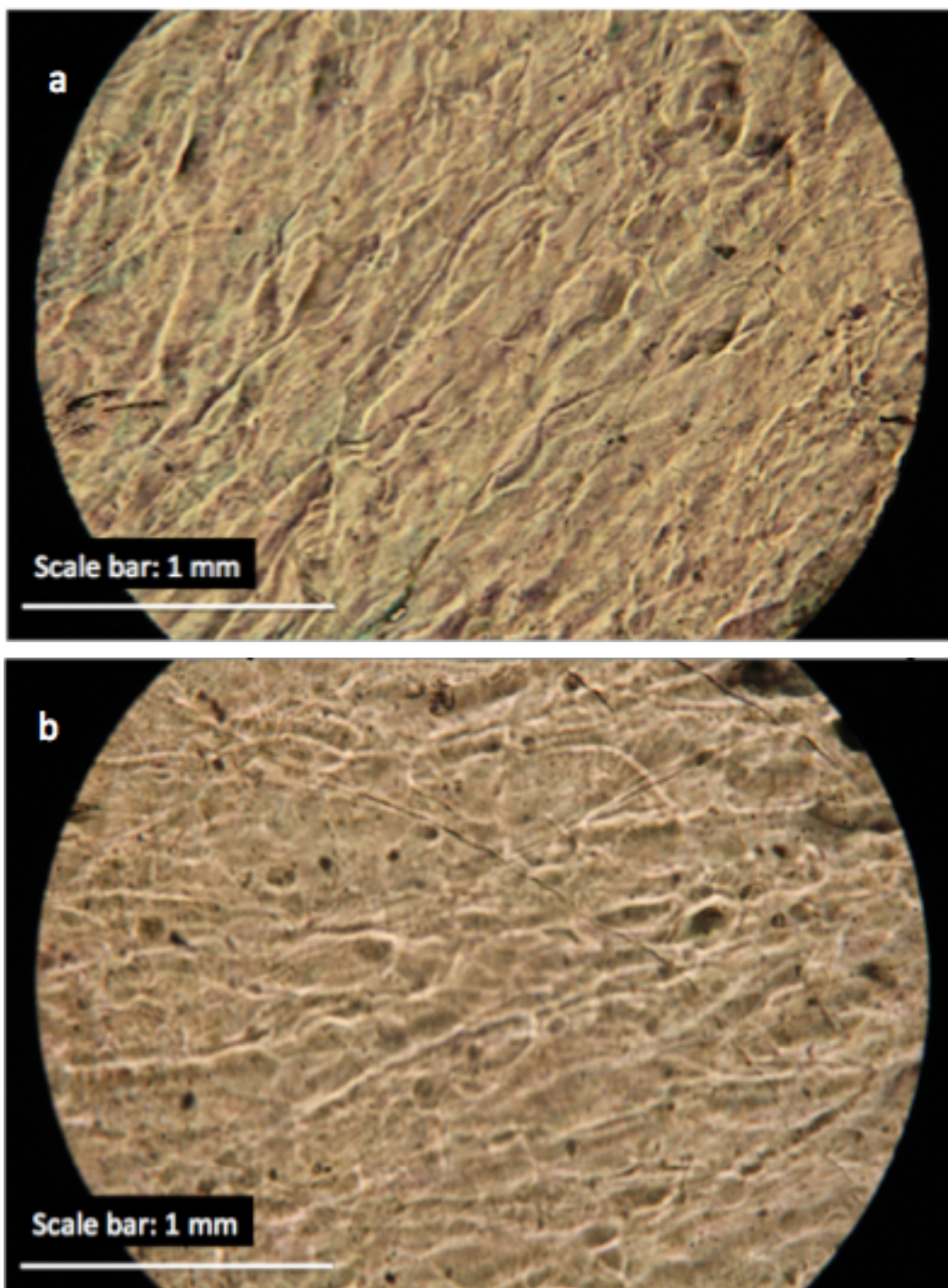


Figure 8. Micrographs of 3.5 wt.% films before (a) and after (b) humidity using non-polarized light.

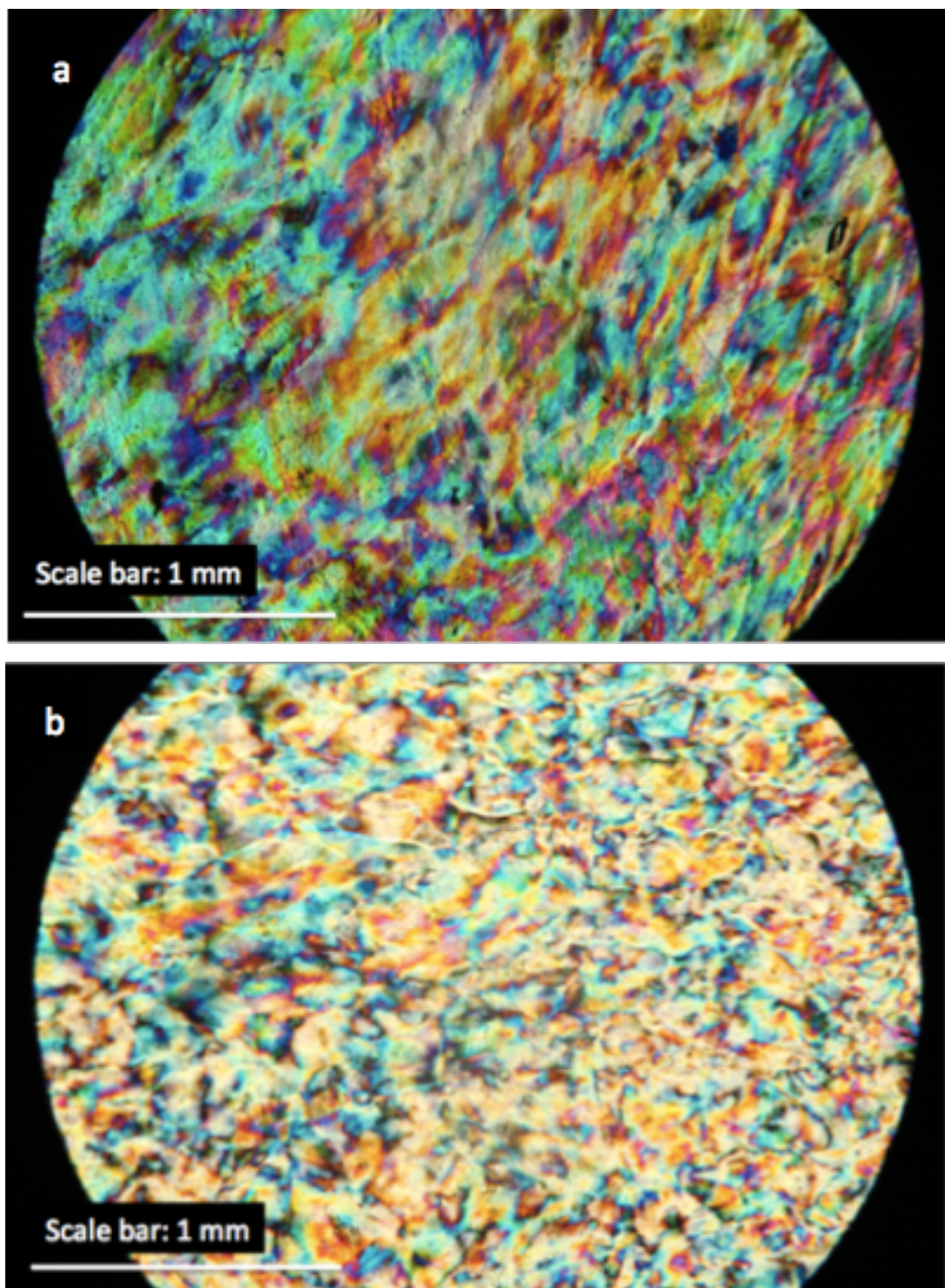


Figure 9. Micrographs of 3.5 wt.% films before (a) and after (b) humidity using polarized light.

3.5 Optical Microscopy Images of 9.1 wt.% Films

Micrographs of 9.1 wt.% films were also taken before and after the DMA experiments were conducted. Both non-polarized (Figure 9) and polarized (Figure 10) light were used to determine what changes happened to the films once exposed to humidity. Figures 9a and 10a show the film before humidity exposure while Figures 9b and 10b show the film after humidity is introduced to the film at both 30°C and 50°C.

The non-polarized images show some differences. The micrograph prior to humidity does not experience much color and is closer to a brown-red shade. Although the 9.1 wt.% solution was ultrasonicated, it may have not been long enough to decrease the pitch length enough to freely space the CNC chains. With a higher concentration, the more likely the chains are to stack together. After humidity, the non-polarized film still shows mostly a brown color, but now there are more tints of blue shown throughout which would mean the pitch length decreased somewhat, and the chains reorganized during the runs.

The polarized micrographs also show differences when it comes to the vibrancy of the colors that appear. Before the film was exposed to humidity in the DMA, the colors are very dark, with more shades of orange and red appearing. After humidity, the films are brighter with shades of red and orange on the outside of the micrograph, but shades of blue throughout the middle.

The pitch length plays an important role in having these features of the micrographs. Although these films were ultrasonicated, the concentration of solid to liquid is very high which makes it harder to orient freely. The pitch length was still affected by the ultrasonication, but having a higher concentration did not allow the CNC chains to align next to each other, but on top of each other initially. This is why the polarized image prior to humidity affect shows darker shades closer to red shades than blue. After the humidity is introduced to the 9.1 wt.% films, the chains align differently on the core of

the films. Closer to the middle of the films, the chains are more freely oriented and adjacent to each other, but continue to position on top of one another on the edges. The temperature effect may also play a vital role in the alignment and pitch length of the CNC chains.

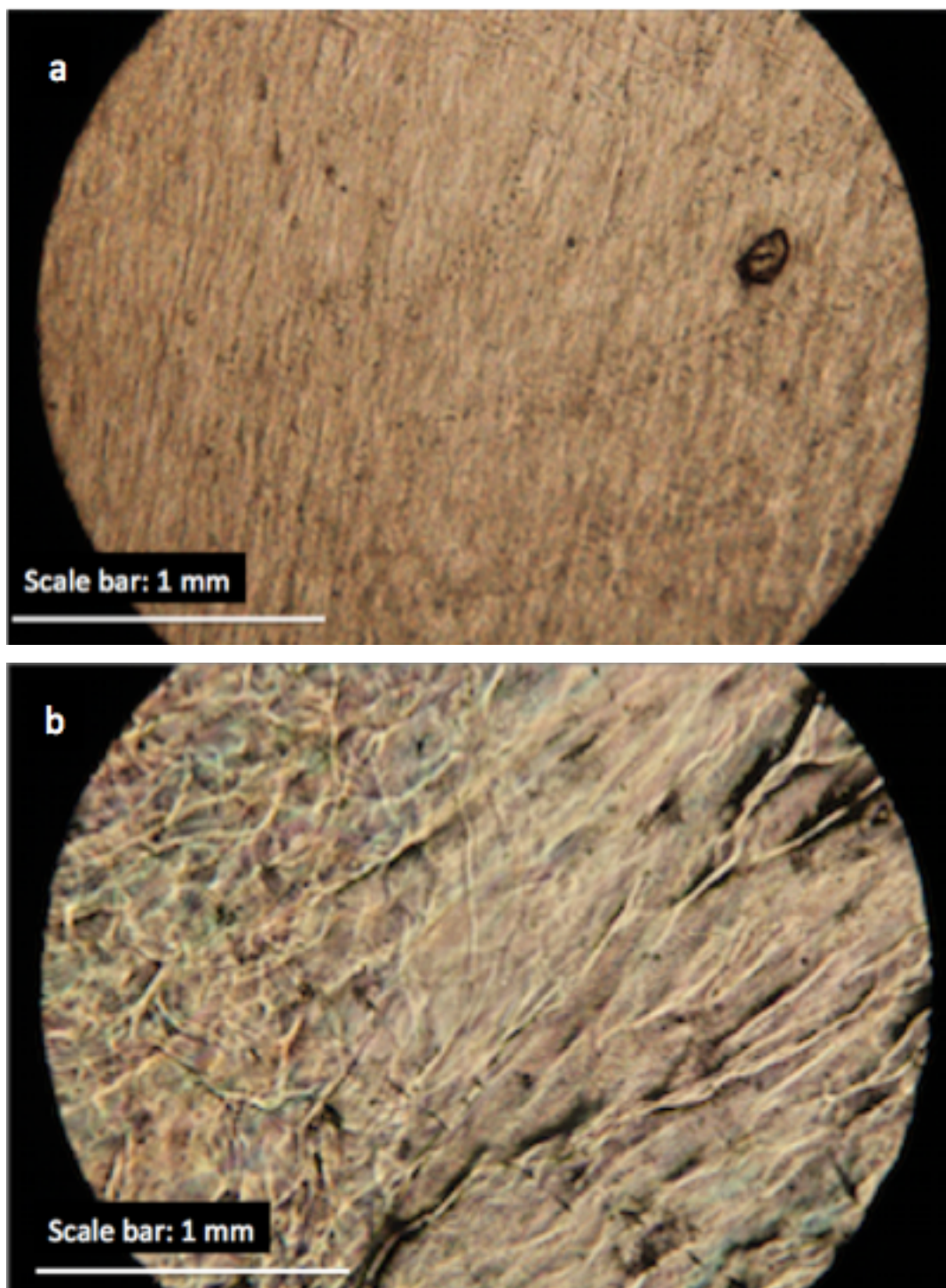


Figure 10. Micrographs of 9.1 wt.% films before (a) and after (b) humidity using non-polarized light.

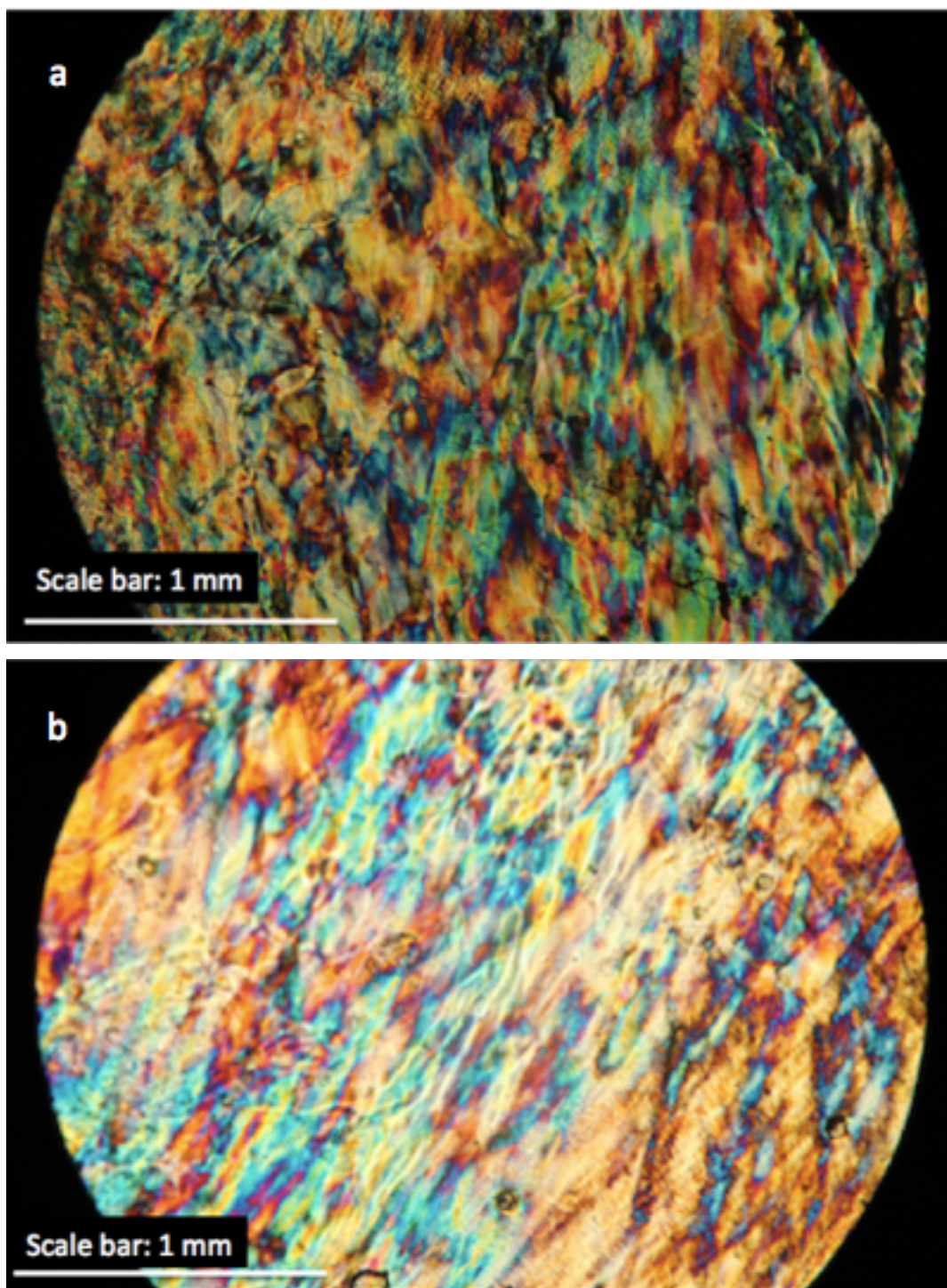


Figure 11. Micrographs of 9.1 wt.% films before (a) and after (b) humidity using polarized light.

3.6 Comparison of 3.5 wt.% and 9.1 wt.% Films Optical Microscopy Images

Sections 3.4 and 3.5 discussed the differences between the non-polarized and polarized images of 3.5 wt.% and 9.1 wt.% films. In this section, the differences observed in the two weight percentages of CNCs will be discussed. As explained, lower concentrations are able to move more freely while drying. This explains the differences in the non-polarized and polarized images before humidity at 3.5 wt.% and 9.1 wt.%. For the first set of films, the chains were able to move freely with a lower pitch length and settle next to each other. This led to a micrograph with more blue colors than the 9.1 wt.% micrograph both with and without polarized light.

Both weight percentages showed changes in the polarized micrographs after the films were introduced to humidity. It can be assumed that the humidity effect plays a role in the pitch length of CNCs and the final structure of the film.

CHAPTER 4. CONCLUSIONS AND FUTURE WORK

The mechanical and optical properties of CNCs can be affected by a variety of parameters. This research shows that the creep response of ultrathin neat-CNC films changes when humidity is introduced. As the humidity is increased to 80% at both 30°C and 50°C, the strain increases. However, as the humidity is decreased to 40%, there is full creep recovery. Finally, there is shrinkage of the film when the humidity is decreased back to 0%. Further research needs to be performed to determine whether this shrinkage of the films is due to the humidity effect or the force effect. The data collected shows that there is a response to the changing humidity effect throughout the experiment. The structural changes of the films are seen in the optical micrographs.

There is also an effect on the optical properties of CNC films due to humidity. First, as reported by other groups, one can see the pitch length is affected by the concentration and ultrasonication of the solutions. However, there is still further shift in color as the films are introduced to humidity. Many more tests can be run to determine this trend.

In the future, films can be made using a multitude of procedures to look at the difference in mechanical and optical properties. Films of the same weight percentages can be placed in an oven to dry within a few hours and then tested using the same DMA method. Optical images can also be taken of these films to see if the polarized images prior to humidity look different than the films that are left to dry at room temperature. It was observed that there were no real differences between the films where the solution was left in the refrigerator after ultrasonication versus the solution being poured directly into the petri dishes. However, there could be a difference in the mechanical and optical

properties. These films can be tested in the future to determine if there are any differences in creep or optical colors.

A method where the humidity is increased at a slower rate could also be run on the films already made and the new ones made to see if the trend is the same. This new method could run the current method backwards, starting at 0% humidity and increasing to 40% and then 80%. Also, higher temperatures, i.e. 70°C and 90°C, could be held while the method runs to determine the changes in creep response.

Finally, additional new testing can be done on the current and future CNC films to further predict certain properties of the neat-CNC films. The optical properties can be looked at by using x-ray diffraction (XRD), scanning electron microscopy (SEM) and circular dichroism (CD) to analyze the pitch lengths of the films prior to and after humidity interaction. Hopefully, these claims would back up the claims made from this research and complement the previous research done on neat-CNC films.

LIST OF REFERENCES

LIST OF REFERENCES

- [1] K. A. Iyer, G. T. Schueneman, and J. M. Torkelson, "Cellulose nanocrystal/polyolefin biocomposites prepared by solid-state shear pulverization: Superior dispersion leading to synergistic property enhancements," *Polym. (United Kingdom)*, vol. 56, pp. 464–475, 2015.
- [2] D. Bondeson, A. Mathew, and K. Oksman, "Optimization of the isolation of nanocrystals from microcrystalline cellulose by acid hydrolysis," *Cellulose*, vol. 13, no. 2, pp. 171–180, 2006.
- [3] T. Saito, S. Kimura, Y. Nishiyama, and A. Isogai, "Cellulose nanofibers prepared by TEMPO-mediated oxidation of native cellulose," *Biomacromolecules*, vol. 8, no. 8, pp. 2485–2491, 2007.
- [4] T. Saito and A. Isogai, "TEMPO-mediated oxidation of native cellulose. The effect of oxidation conditions on chemical and crystal structures of the water-insoluble fractions," *Biomacromolecules*, vol. 5, no. 5, pp. 1983–1989, 2004.
- [5] N. Lavoine, I. Desloges, A. Dufresne, and J. Bras, "Microfibrillated cellulose - Its barrier properties and applications in cellulosic materials: A review," *Carbohydr. Polym.*, vol. 90, no. 2, pp. 735–764, 2012.
- [6] L. Brinchi, F. Cotana, E. Fortunati, and J. M. Kenny, "Production of nanocrystalline cellulose from lignocellulosic biomass: Technology and applications," *Carbohydr. Polym.*, vol. 94, no. 1, pp. 154–169, 2013.
- [7] Y. Habibi, L. A. Lucia, and O. J. Rojas, "Cellulose nanocrystals: Chemistry, self-assembly, and applications," *Chem. Rev.*, vol. 110, no. 6, pp. 3479–3500, 2010.
- [8] J. Yang, C. R. Han, J. F. Duan, M. G. Ma, X. M. Zhang, F. Xu, and R. C. Sun, "Synthesis and characterization of mechanically flexible and tough cellulose nanocrystals-polyacrylamide nanocomposite hydrogels," *Cellulose*, vol. 20, no. 1, pp. 227–237, 2013.
- [9] J. A. Diaz, X. Wu, A. Martini, J. P. Youngblood, and R. J. Moon, "Thermal expansion of self-organized and shear-oriented cellulose nanocrystal films," *Biomacromolecules*, vol. 14, no. 8, pp. 2900–2908, 2013.

- [10] A. B. Reising, R. J. Moon, and J. P. Youngblood, "Development, Processing and Characterization of Cellulose Nanocrystal Neat Films," *J. Sci. Technol. For. Prod. Process.*, 2013.
- [11] V. Landry, A. Alemdar, and P. Blanchet, "Nanocrystalline Cellulose : Morphological , Physical , and Mechanical Properties," vol. 61, no. 10, pp. 104–112, 2011.
- [12] R. J. Moon, A. Martini, J. Nairn, J. Simonsen, and J. Youngblood, *Cellulose nanomaterials review: structure, properties and nanocomposites*, vol. 40, no. 7. 2011.
- [13] Y. Habibi, L. a Lucia, and O. J. Rojas, "Cellulose Nanocrystals : Chemistry , Self-Assembly , and Applications," *Chem. Rev.*, vol. 110, pp. 3479–3500, 2009.
- [14] M. Mariano, N. El Kissi, and A. Dufresne, "Cellulose nanocrystals and related nanocomposites: Review of some properties and challenges," *J. Polym. Sci. Part B Polym. Phys.*, vol. 52, no. 12, pp. 791–806, 2014.
- [15] V. Favier, H. Chanzy, and J. Y. Cavaille, "Nanocomposite materials from latex and cellulose whiskers," *Polym. Advanved Technol.*, vol. Volume 6, pp. 365–367, 1996.
- [16] Y. Zhou, C. Fuentes-Hernandez, T. M. Khan, J.-C. Liu, J. Hsu, J. W. Shim, A. Dindar, J. P. Youngblood, R. J. Moon, and B. Kippelen, "Recyclable organic solar cells on cellulose nanocrystal substrates.," *Sci. Rep.*, vol. 3, p. 1536, 2013.
- [17] R. M. A. Domingues, M. E. Gomes, and R. L. Reis, "The potential of cellulose nanocrystals in tissue engineering strategies," *Biomacromolecules*, vol. 15, no. 7. pp. 2327–2346, 2014.
- [18] W. Li, R. Guo, Y. Lan, Y. Zhang, W. Xue, and Y. Zhang, "Preparation and properties of cellulose nanocrystals reinforced collagen composite films," *J. Biomed. Mater. Res. - Part A*, vol. 102, no. 4, pp. 1131–1139, 2014.
- [19] P. Dhar, U. Bhardwaj, A. Kumar, and V. Katiyar, "Poly (3-hydroxybutyrate)/Cellulose Nanocrystal Films for Food Packaging Applications: Barrier and Migration Studies," *Polym. Eng. Sci.*, vol. 55, pp. 2388–2395, 2015.
- [20] T. S. Yoshiharu Doi, Youko Kanesawa, Masao Kunioka, "Biodegradation of microbial copolyesters: poly(3-hydroxybutyrate-co-3-hydroxyvalerate) and poly(3-hydroxybutyrate-co-4-hydroxybutyrate)," *Macromolecules*, vol. 23, no. 1, pp. 26–31, 1990.

- [21] D. Wu, L. Wu, L. Wu, and M. Zhang, "Rheology and thermal stability of polylactide/clay nanocomposites," *Polym. Degrad. Stab.*, vol. 91, no. 12, pp. 3149–3155, 2006.
- [22] J. R. Fried, *Polymer Science and Technology*, 2nd ed. Upper Saddle River, NJ: Prentice Hall Professional Technical Reference, 2003.
- [23] F. Mainardi and G. Spada, "Creep, relaxation and viscosity properties for basic fractional models in rheology," *Eur. Phys. J. Spec. Top.*, vol. 193, no. 1, pp. 133–160, 2011.
- [24] S. Qi, M. Yu, J. Fu, P. D. Li, and M. Zhu, "Creep and recovery behaviors of magnetorheological elastomer based on polyurethane / epoxy resin IPNs matrix," *Smart Mater. Struct.*, vol. 25, pp. 1–10, 2016.
- [25] J. Zhao and A. R. Barron, *Dynamic mechanical analysis*, vol. 9. 2014.
- [26] F. Jin, Z. Jiang, and Q. Wu, "Creep Behavior of Wood Plasticized by Moisture and Temperature," *BioResources*, vol. 11, no. 1, pp. 827–838, 2016.
- [27] P. Navi, V. Pittet, and C. J. G. Plummer, "Transient moisture effects on wood creep," *Wood Sci. Technol.*, vol. 36, no. 6, pp. 447–462, 2002.
- [28] A. Ranta-Maunus, "The viscoelasticity of wood at varying moisture content," *Wood Sci. Technol.*, vol. 9, no. 3, pp. 189–205, 1975.
- [29] S. Spoljaric, A. Genovese, and R. A. Shanks, "Polypropylene-microcrystalline cellulose composites with enhanced compatibility and properties," *Compos. Part A Appl. Sci. Manuf.*, vol. 40, no. 6–7, pp. 791–799, 2009.
- [30] A. Ashori, "Wood-plastic composites as promising green-composites for automotive industries!," *Bioresour. Technol.*, vol. 99, no. 11, pp. 4661–4667, 2008.
- [31] M. Bengtsson, P. Gatenholm, and K. Oksman, "The effect of crosslinking on the properties of polyethylene/wood flour composites," *Compos. Sci. Technol.*, vol. 65, no. 10, pp. 1468–1479, 2005.
- [32] S. Y. Lee, H. S. Yang, H. J. Kim, C. S. Jeong, B. S. Lim, and J. N. Lee, "Creep behavior and manufacturing parameters of wood flour filled polypropylene composites," *Compos. Struct.*, vol. 65, no. 3–4, pp. 459–469, 2004.

- [33] A. K. Bledzki and O. Faruk, "Creep and impact properties of wood fibre-polypropylene composites: Influence of temperature and moisture content," *Compos. Sci. Technol.*, vol. 64, no. 5, pp. 693–700, 2004.
- [34] L. Sobczak, R. W. Lang, and A. Haider, "Polypropylene composites with natural fibers and wood - General mechanical property profiles," *Compos. Sci. Technol.*, vol. 72, no. 5, pp. 550–557, 2012.
- [35] M. L. Auad, V. S. Contos, S. Nutt, M. I. Aranguren, and N. E. Marcovich, "Characterization of nanocellulose-reinforced shape memory polyurethanes," *Polymer International*, vol. 57, no. 10, pp. 651–659, 2008.
- [36] X. Liu, R. D. Wildman, and I. A. Ashcroft, "Experimental investigation and numerical modelling of the effect of the environment on the mechanical properties of polyurethane lacquer films," *J. Mater. Sci.*, vol. 47, no. 13, pp. 5222–5231, 2012.
- [37] A. J. Nolte, N. D. Treat, R. E. Cohen, and M. F. Rubner, "Effect of relative humidity on the Young's modulus of polyelectrolyte multilayer films and related nonionic polymers," *Macromolecules*, vol. 41, no. 15, pp. 5793–5798, 2008.
- [38] E. Niinivaara, M. Faustini, T. Tammelin, and E. Kontturi, "Water vapor uptake of ultrathin films of biologically derived nanocrystals: Quantitative assessment with quartz crystal microbalance and spectroscopic ellipsometry," *Langmuir*, vol. 31, no. 44, pp. 12170–12176, 2015.
- [39] J. A. Kelly, M. Giese, K. E. Shopsowitz, W. Y. Hamad, and M. J. MacLachlan, "The development of chiral nematic mesoporous materials," *Acc. Chem. Res.*, vol. 47, no. 4, pp. 1088–1096, 2014.
- [40] X. M. Dong and D. G. Gray, "Effect of Counterions on Ordered Phase Formation in Suspensions of Charged Rodlike Cellulose Crystallites," *Langmuir*, vol. 13, no. 8, pp. 2404–2409, 1997.
- [41] S. Beck, J. Bouchard, and R. Berry, "Controlling the reflection wavelength of iridescent solid films of nanocrystalline cellulose," *Biomacromolecules*, vol. 12, no. 1, pp. 167–172, 2011.
- [42] J. Pan, W. Hamad, and S. K. Straus, "Parameters affecting the chiral nematic phase of nanocrystalline cellulose films," *Macromolecules*, vol. 43, no. 8, pp. 3851–3858, 2010.

- [43] A. M. Ritcey, G. Charlet, and D. G. Gray, "Effect of residual linear orientation on the optical properties of cholesteric films," *Can. J. Chem.*, vol. 66, pp. 2229–2233, 1988.
- [44] A. M. Ritcey and D. G. Gray, "Circular reflectivity from the cholesteric liquid crystalline phase of (2-ethoxypropyl)cellulose," *Macromolecules*, vol. 21, no. 5, pp. 1251–1255, 1988.
- [45] G. Jian-Xin and G. Derek G., "Chiroptical Behavior of (Acetyl) (ethyl)cellulose Liquid Crystalline Solutions in Chloroform," *Macromolecules*, vol. 22, pp. 2086–2090, 1989.